

Non-normal growth in symmetric shear flow

Eyal Heifetz^a and Brian F. Farrell^b

^a*Department of Geophysics and Planetary Sciences, Tel-Aviv University, Israel*

^b*Department of Earth and Planetary Sciences, Harvard University, Cambridge, Mass., USA*

ABSTRACT: An analysis of symmetric instability from the perspective of Generalized Stability Theory is presented. For Richardson number smaller than one, the optimal growth exceeds that predicted by normal mode analysis yielding potentially a much faster generation of slantwise convection. In both normal and non-normal evolution, the parcel trajectory remains close to the isentropes and energy growth results primarily from the vertical Reynolds stress term in the energy equation. The large non-normal growth obtained results from the optimal perturbations having parcel trajectories in the mean shear plane, in the initial stage, that maximize the growth by Reynolds stress. This plane is perpendicular to the plane of the isentropes and the absolute momentum isolines, usually associated with slantwise convection. For Richardson number larger than unity, transient growth results primarily from the meridional heat flux term in the energy equation, however this growth is relatively small. Copyright © 2008 Royal Meteorological Society

KEY WORDS Generalized Stability Theory; slantwise convection; Reynolds stress

Received 8 January 2008; Revised 23 June 2008; Accepted 11 July 2008

1. Introduction

Symmetric Instability (SI) resulting in slantwise convection is considered to be an important mechanism of rain bands formation in frontal regions. A thorough review (together with a rich reference list) of different types of SI and the ‘use and misuse’ of them appears in Schultz and Schumacher (1999). Theoretical treatment of linear SI dynamics (Stone, 1966, 1970; Hoskins, 1974; Bennetts and Hoskins, 1979; Emanuel, 1983a,b; Xu, 1986a,b) focused mainly on normal mode analysis, in which attention was focused on the necessary Richardson number condition for instability, and on the largest modal growth rate as a measure of the potential for occurrence of slantwise convection.

However, shear flow in general is non-normal, e.g. Farrell (1984), in the sense that the normal modes are not orthogonal. As a result, an initial perturbation can transiently grow even if all normal modes are stable. Furthermore, if unstable normal modes exist one can almost always find a transiently growing perturbation with growth rate exceeding the growth rate of the most unstable mode. The Generalized Stability Theory (GST) derived by Farrell and Ioannou (1996, hereafter FI96) shows how a Singular Value Decomposition (SVD) of the propagator matrix of the linearized dynamical equation determines the optimal evolution which yields the largest possible growth in a given target time.

Recently, Heifetz and Farrell (2007) examined the GST for non-geostrophic baroclinic shear flows for Richardson

numbers of order one, however they did not analyze the symmetric instability since the focus of that work (continuing an analysis for large Richardson number regime; Heifetz and Farrell, 2003) was on the loss of orthogonality between Rossby and gravity waves. In this note we look at non-normal optimal growth of SI for $Ri = O(0.1 - 1)$. While recognizing the fundamental role of moisture in the development of rain bands, we concentrate here on the simplest dry SI version in order to examine the essence of non-normality in this system.

In section 2 we formulate the problem, then examine the normal versus the optimal non-normal perturbation growth in section 3, and conclude our results in section 4.

2. Formulation

Consider a Boussinesq, quasi-hydrostatic basic state with constant vertical shear $\partial U/\partial z = \Lambda$, on an f plane. Both the basic state and the perturbations are assumed to be constant in the zonal direction x . The linearized momentum, thermodynamic and continuity equations for zonally symmetric perturbations are:

$$\dot{u} = fv - \Lambda w, \quad (1a)$$

$$\dot{v} = -fu - \frac{\partial p}{\partial y}, \quad (1b)$$

$$\theta - \frac{\partial p}{\partial z} = 0, \quad (1c)$$

$$\dot{\theta} = f\Lambda v - N^2 w, \quad (1d)$$

$$\frac{\partial v}{\partial y} + \frac{\partial w}{\partial z} = 0, \quad (1e)$$

*Correspondence to: Eyal Heifetz, Dept. of Geophysics and Planetary Sciences, Tel-Aviv University, Israel. Email: eyalh@cyclone.tau.ac.il

in which (u, v, w) are the perturbation velocity components in the (x, y, z) directions, $\theta = (g/\theta_0)\theta'$ is the perturbation scaled potential temperature and the perturbation pressure p is scaled by an assumed constant density, $N^2 = (g/\theta_0)(\partial\Theta/\partial z)$ is the Brunt–Väisälä frequency and the basic state is in thermal wind balance, $f\Lambda = -(g/\theta_0)(\partial\Theta/\partial y)$. Note that, since there is no mean shear in the meridional direction, the meridional derivative of the absolute momentum, $M = fy - U(z)$, is simply the Coriolis parameter f .

For periodic perturbations in the meridional and vertical directions, (1) yields the energy equation:

$$\begin{aligned} \dot{E} &= \frac{\partial}{\partial t} \int_y \int_z \frac{1}{2} \left[u^2 + v^2 + \left(\frac{\theta}{N} \right)^2 \right] dydz \\ &= \Lambda \int_y \int_z \left(\frac{f}{N^2} v\theta - uv \right) dydz, \end{aligned} \tag{2}$$

where the terms on the RHS are the meridional heat flux and the vertical Reynolds stress sources for potential and kinetic energy growth, respectively.

We look for plane wave perturbations of the form $e^{i(l y + m z)}$ so we can write (1a,b,d), with the aid of (1c,e) as:

$$\dot{u} = \left(f + \frac{l}{m} \Lambda \right) v, \tag{3a}$$

$$\dot{v} = -f u - \frac{l}{m} \theta, \tag{3b}$$

$$\dot{\theta} = \left(f \Lambda + \frac{l}{m} N^2 \right) v. \tag{3c}$$

Next, we non-dimensionalize time by f^{-1} , horizontal and vertical distance by L and H , and velocity and $\eta = (\theta/N)$ by U . Denoting the aspect ratio by $\alpha = H/L$, the effective Rossby, Richardson and Burger numbers can be written as:

$$Ro = \frac{U}{fL} = \alpha \frac{\Lambda}{f}, \tag{4a}$$

$$Ri = \left(\frac{N}{\Lambda} \right)^2, \tag{4b}$$

$$Br = \left(\alpha \frac{N}{f} \right)^2 = Ro^2 Ri. \tag{4c}$$

Equation set (3) can now be rewritten as:

$$\dot{u} = \left(1 + \frac{l}{m} Ro \right) v, \tag{5a}$$

$$\dot{v} = -u - \frac{l}{m} \sqrt{Br} \eta, \tag{5b}$$

$$\dot{\eta} = \left(\frac{1}{\sqrt{Ri}} + \frac{l}{m} \sqrt{Br} \right) v. \tag{5c}$$

The non-dimensional energy equation (2) becomes

$$\dot{E} = \frac{1}{\sqrt{Ri}} \int_y \int_z \left(\eta v + \sqrt{Br} \frac{l}{m} uv \right) dydz. \tag{6}$$

While both the energy sources are proportional to $1/\sqrt{Ri}$, the ratio between the vertical Reynolds stress and the meridional heat flux is proportional to \sqrt{Br} .

Equation (5) can be written in the matrix form:

$$\dot{\mathbf{e}} = \mathbf{A} \mathbf{e}, \tag{7}$$

where the normalized energy coordinate vector, \mathbf{e} , and the matrix \mathbf{A} are:

$$\mathbf{e} = \begin{pmatrix} u \\ v \\ \eta \end{pmatrix}, \quad \mathbf{A} = \begin{pmatrix} 0 & (1 + \frac{l}{m} Ro) & 0 \\ -1 & 0 & -\frac{l}{m} \sqrt{Br} \\ 0 & \left(\frac{1}{\sqrt{Ri}} + \frac{l}{m} \sqrt{Br} \right) & 0 \end{pmatrix}. \tag{8}$$

3. Normal and non-normal growth

3.1. Normal growth

The three eigenvalues of \mathbf{A} are:

$$\lambda_{1,2} = \pm i \left[\left(\frac{l}{m} \right)^2 Br + 2 \frac{l}{m} Ro + 1 \right]^{1/2}, \quad \lambda_3 = 0. \tag{9}$$

Hence, in order to have modal instability, (l/m) must be negative, i.e. the normal modes are tilted northward with height, as expected. (The absolute momentum isolines and the isentropes are also tilted northward with height.) With the definition $\chi \equiv |l/m|$, the condition for instability (to obtain positive real λ) is therefore

$$\begin{aligned} Br \chi^2 - 2Ro \chi + 1 &< 0 \\ \implies \frac{Ro}{Br} [1 - \sqrt{1 - Ri}] &< \chi < \frac{Ro}{Br} [1 + \sqrt{1 - Ri}], \end{aligned} \tag{10a, 10b}$$

and since χ must be real, this implies the well-known condition for modal instability $Ri < 1$. The largest modal growth rate $\lambda_{nm-\max} = \sqrt{1/Ri - 1}$, is obtained when $\chi = Ro/Br$, that is when the perturbation slope $\alpha\chi = \alpha Ro/Br = f\Lambda/N^2 = \tan \gamma_\Theta$, where $\tan \gamma_\Theta$ is the mean isentrope slope. (Recall that the mean absolute momentum slope $\tan \gamma_M = f/\Lambda$, therefore $\tan \gamma_M / \tan \gamma_\Theta = Ri$. Hence, to obtain modal symmetric instability, the slope of the isentropes should exceed the slope of the absolute momentum isolines).

For this case of $\chi = Ro/Br$ the growing, decaying and neutral normal modes become

$$\mathbf{e}_g = \sqrt{Ri} \begin{pmatrix} 1 \\ -\sqrt{\frac{1}{Ri} - 1} \\ 0 \end{pmatrix}, \tag{11a}$$

$$\mathbf{e}_d = \sqrt{Ri} \begin{pmatrix} 1 \\ \sqrt{\frac{1}{Ri} - 1} \\ 0 \end{pmatrix}, \tag{11b}$$

$$\mathbf{e}_n = \frac{1}{\sqrt{1 + Ri}} \begin{pmatrix} 1 \\ 0 \\ \sqrt{Ri} \end{pmatrix}. \tag{11c}$$

The most unstable mode has zero potential temperature perturbation. (This is a degenerate property of the most unstable mode due to the hydrostatic approximation used here for the sake of simplicity. As was shown by Xu and Zhou (1982), this degenerate property is seen only in the hydrostatic limit. Without the hydrostatic approximation, the most unstable mode will have non-zero potential temperature perturbation yielding air parcel slope to be much less steep than the isentrope slopes, cf. Xu and Clark, 1985.) Therefore, according to (6), all of the unstable mode energy growth results from the vertical Reynolds stress. The decaying mode is the complex conjugate of the growing mode. The neutral mode has non-zero potential temperature but zero meridional velocity. Therefore it cannot exhibit growth, neither from the meridional heat flux, nor from the vertical Reynolds stress. According to (1e), the neutral mode has no vertical circulation. Hence, the zonal velocity perturbation and potential temperature perturbation in the neutral mode are stationary and satisfy the thermal-wind balance (11c).

The unstable, decaying and neutral modes are not orthogonal in general and this leaves open the possibility of transient growth. λ_{nm-max} is plotted as a function of Ri in Figure 1(a). The inner product between the three modes of (11) is plotted in Figure 1(b). The growing and the decaying normal modes are parallel

when the Richardson number is zero and one, and perpendicular when $Ri = 0.5$. The non-orthogonality between the growing or the decaying mode (one is the complex conjugate of the other) with the neutral mode is maximized at zero Richardson number (at which the modes become parallel) and decays to zero (the modes are perpendicular) for unit Richardson number. The three vectors are plotted, for $Ri = 0.5$, in Figure 1(d), where the orthogonality between the unstable and decaying modes is clearly seen. In the stable regime the growing and decaying normal modes become neutral but preserve a zero potential temperature signature and become more orthogonal as Ri increases. Apart from the ill-posed solution at $Ri = 1$ (when the three modes are parallel) the third neutral mode is perpendicular to the other modes in the neutral regime (Figure 1(b)).

3.2. Non-normal growth

Due to the non-orthogonality among the modes, the matrix A is generally non-normal, and this implies that transient growth occurs in the modal stable regime $Ri > 1$, and that the optimal growth, when $Ri < 1$, is greater than the most unstable modal growth rate λ_{nm-max} . According to FI96, the greatest instantaneous growth rate is the largest eigenvalue of the matrix

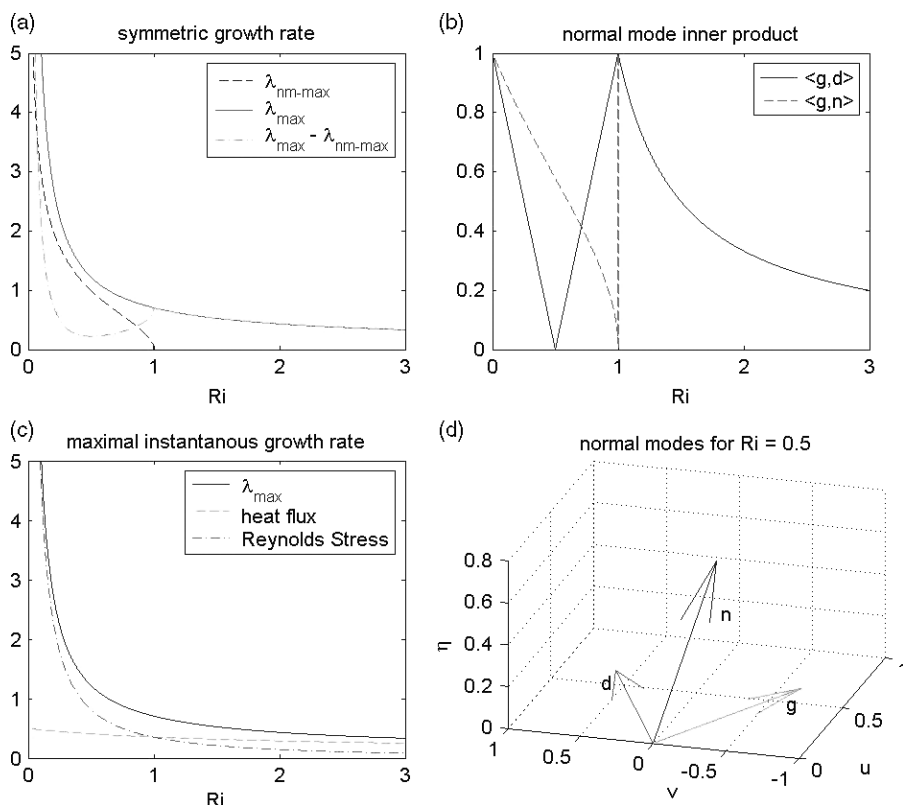


Figure 1. (a) The most unstable normal mode growth rate (dashed), the largest instantaneous growth rate (solid), and their difference (dash-dot), as a function of the Richardson number. (b) Energy norm inner product between the three normal modes, as a function of the Richardson number. The inner product between the growing and decaying normal modes (solid), and between the growing and the neutral modes (dashed). (The latter is also equal to the inner product between the decaying and the neutral modes.) When $Ri = 1$, the three modes are parallel. (c) The largest instantaneous growth rate (solid) composed of the meridional heat flux (dashed) and the vertical Reynolds stress (dash-dot) components. (d) A visual example of the three normal mode vectors in the generalized energy coordinates space for $Ri = 0.5$. This figure is available in colour online at www.interscience.wiley.com/journal/qj

$(\mathbf{A} + \mathbf{A}^\dagger)/2$, when $(l/m) < 1$:

$$\frac{1}{2}(\mathbf{A} + \mathbf{A}^\dagger) = \frac{1}{2} \begin{pmatrix} 0 & -Ro\chi & 0 \\ -Ro\chi & 0 & \frac{1}{\sqrt{Ri}} \\ 0 & \frac{1}{\sqrt{Ri}} & 0 \end{pmatrix}, \quad (12)$$

which is equal to $\lambda_{\max} = \frac{1}{2}\sqrt{(Br\chi^2 + 1)/Ri}$. We focus here on the configurations that provide the largest modal growth, i.e. when $\chi = Ro/Br$, and explore its non-modal growth. In Figure 1(a), λ_{\max} is plotted for comparison with $\lambda_{\text{nm-max}}$, together with the difference between these growth rates. In the unstable regime, the maximal instantaneous growth rate is indeed larger than the modal growth rate. Their difference is minimized when $Ri = 0.5$, where the growing and decaying modes are orthogonal. In the stable regime λ_{\max} is rather small (for instance for $Ri = 5$, $\lambda_{\max} \approx 0.25 \approx 1/7$ hours in dimensional units) and in the stable regime this growth is not sustained, since the optimal evolution vacillates between the three neutral modes. The global optimal, that is the largest energy amplification the perturbation can achieve for any time, is smaller than a factor 5 even close to Richardson number unity (at $Ri = 1.1$, Figure 2(d)), and decays rapidly as Richardson number increases.

The instantaneous amplitude growth in the energy norm is

$$\lambda_{\text{inst}} = \frac{\dot{E}}{2E} = \frac{1}{2E} \int_y \int_z \left(\frac{\eta v}{\sqrt{Ri}} - \frac{uv}{Ri} \right) dydz, \quad (13)$$

for $\chi = Ro/Br$. In Figure 1(c), λ_{\max} is decomposed into its two sources – heat flux and Reynolds stress (the two sources on the RHS of (13)). For small Richardson numbers, the Reynolds stress source is clearly dominant, however the two sources become equal for $Ri = 1$ and the heat flux dominates as Richardson number increases further. While the maximal instantaneous growth rate can be large, it still remains to be determined whether this growth can be sustained. The optimal growth for increasing target times is shown in Figure 2 (recall that the time is scaled by f^{-1} so a time unit corresponds approximately to three hours in the midlatitudes) and compare it with the largest exponential modal growth for selected Richardson numbers ($Ri = 0.1, 0.5, 0.9, 1.1$). The largest growth for a given target time is given by the first singular value, σ_1 , of the propagator matrix $e^{\mathbf{A}t}$ which solves (7), cf. FI96. It is clear from Figure 2 that the optimal growth significantly exceeds the modal growth in the unstable regime. In the neutral regime, even very close to the stability boundary, the amplification is small, since the non-normal growth cannot project on an unstable growing mode and so sustain its growth (cf. the

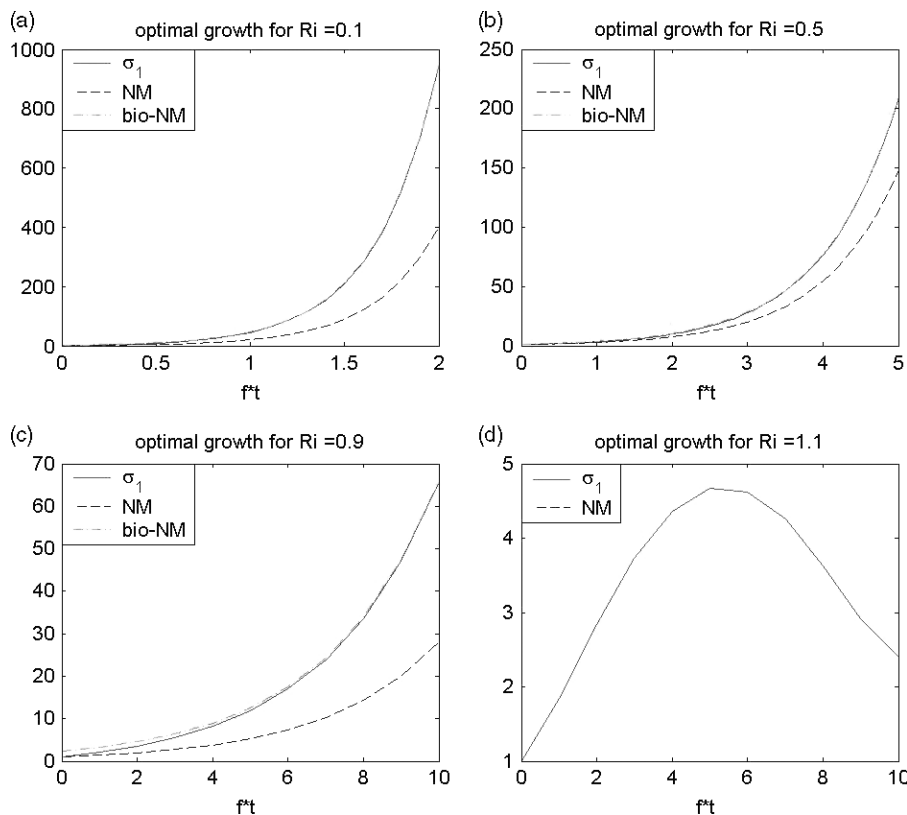


Figure 2. The optimal growth, $\sigma_1(t)$ (solid), the most unstable normal mode growth (dashed) and the growth of its biorthogonal vector (dash-dot) obtained for consecutive non-dimensionalized time intervals ft ($ft = 1$ corresponds approximately to three hours) are shown for $Ri =$ (a) 0.1, (b) 0.5, (c) 0.9 and (d) 1.1. For $Ri = 1.1$, the unstable normal mode, and hence its biorthogonal vector, do not exist. This figure is available in colour online at www.interscience.wiley.com/journal/qj

difference in growth between the two sides of the stability cut-off, i.e. in $Ri = 0.9$ versus in $Ri = 1.1$.

In order to verify the last point, we also address in Figure 2 the ‘infinite’ target time limit of optimal growth. According to FI96, the growth rate at large times converges to that of the most unstable mode, however this exponential growth is multiplied by the magnitude of the biorthogonal vector of the most unstable mode (that in non-normal systems is always larger than one). For large times the optimal initial perturbation is the biorthogonal of the most unstable mode that evolves into the structure of the most unstable mode. The unstable mode growth, multiplied by the magnitude of its biorthogonal vector is indicated by the dash-dot lines in Figure 2. We see that the optimal evolutions converge very quickly to these ‘infinite target time limits’, indicating that the large non-normal evolution occurs at the initial stage of growth. In the stable regime (Figure 2(d)), this non-normal growth cannot be projected on an unstable mode and therefore the growth that is attained is not sustained.

The evolution of the instantaneous growth rate during the optimal growth from the initial biorthogonal perturbation to non-dimensional target times $t = 2, 5, 10$ for $Ri = 0.1, 0.5, 0.9$, respectively, are indicated by the plus symbols in Figure 3. Indeed, most of the growth rate that greatly exceeds the unstable growth rate (indicated by the horizontal solid line) occurs at the initial stage of the

evolution. The instantaneous growth rate is decomposed, according to (13), into meridional heat flux and vertical Reynolds stress components. For small Richardson numbers the optimal growth rate at the initial time of the evolution is dominated by the Reynolds stress, however as Richardson number approaches unity the relative contribution of the meridional heat flux increases. For the example in the stable regime ($Ri = 1.1$, Figure 3(d)) we examine the optimal evolution for non-dimensional target time 5 (the global optimal time). This optimal perturbation for finite time (the first singular vector, \mathbf{V}_1 , of the matrix \mathbf{V} , where $\mathbf{U}\Sigma\mathbf{V}^\dagger = e^{5f\mathbf{A}}$, is the singular value decomposition) is not the biorthogonal vector of the first singular vector of \mathbf{U} . The evolution of the instantaneous growth rate of the vector $e^{\mathbf{A}t}\mathbf{V}_1$ is decomposed into energy source components showing the dominance of the meridional heat flux over the vertical Reynolds stress component. Only for the second global optimal does the Reynolds stress dominate, but these growths are quite small.

The dynamics discussed above focus on the case of perturbation displacement along the isentropes which therefore have no initial potential temperature perturbation. As shown by Hoskins (1974) this is the structure of modal perturbations and therefore a growing normal mode must have zero potential temperature (all fields if non-zero must grow). This is not true for non-normal

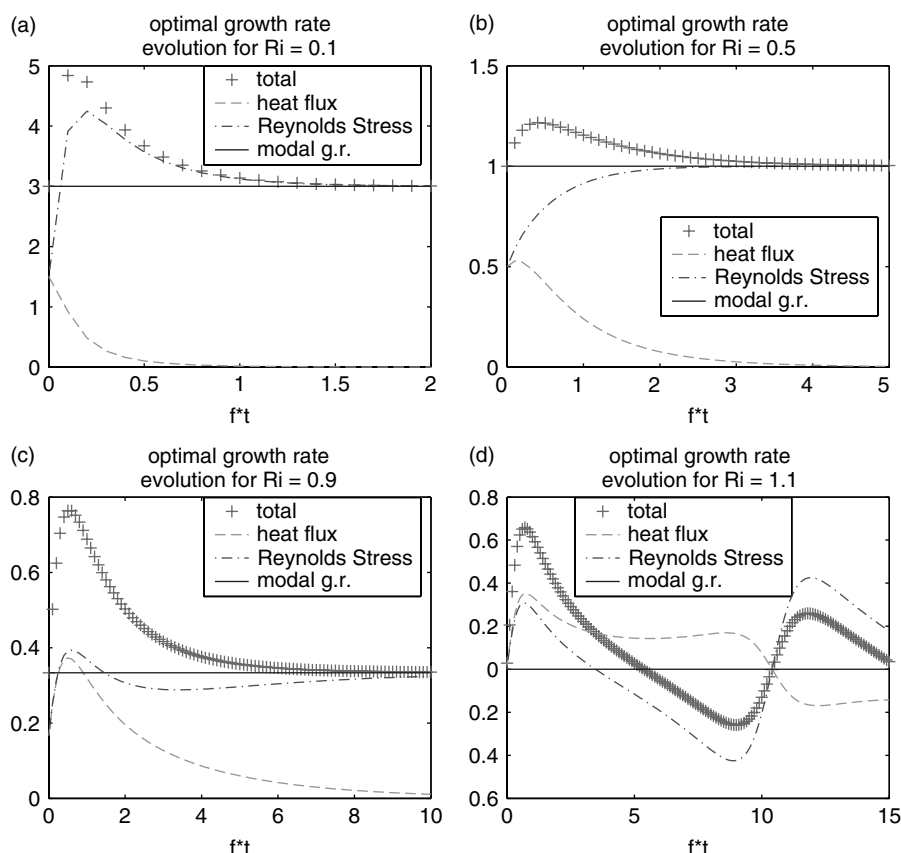


Figure 3. The evolution of the instantaneous growth rate for $Ri =$ (a) 0.1, (b) 0.5, (c) 0.9 and (d) 1.1 during the optimal growth from the initial biorthogonal perturbation to non-dimensional target times 2, 5, 10, 15 respectively. The growth rate is indicated by plus symbols, meridional heat flux by the dashed lines and vertical Reynolds stress components by the dash-dot lines. The most unstable growth rate is indicated for reference by the horizontal solid line. This figure is available in colour online at www.interscience.wiley.com/journal/qj

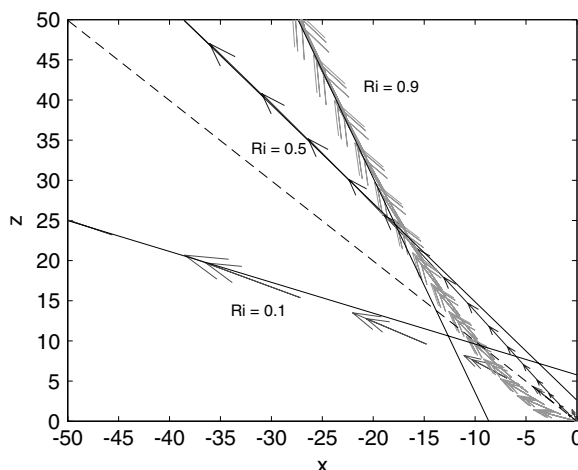


Figure 4. Optimal trajectories (arrows) of air parcels in the (x, z) plane for the cases of $Ri = 0.1, 0.5, 0.9$ until they converge to the constant slope of the unstable modes (indicated by the solid lines). The optimal slope (scaled by Ro/Br) to maximize the Reynolds stress is indicated by the dashed line. The optimal evolution seeks to pass through this slope at the initial time of evolution. This figure is available in colour online at www.interscience.wiley.com/journal/qj

growth in which the meridional heat flux $v\theta$ can evolve with time. Optimal evolution for cases with $Ri < 1$ and the slope of the perturbation taken between the mean isentropes and the absolute momentum isolines were also examined (not shown). While the role of the meridional heat flux is greater in these cases, the optimal growth is smaller since the evolution rapidly converges on an unstable mode which has a smaller growth rate than the gravest unstable mode.

The common interpretation of symmetric instability is made by looking at the (y, z) plane, in which the perturbation and the mean flow are independent of the zonal direction. Nevertheless, in both normal and non-normal growth, the main energy source is the vertical Reynolds stress term $-uw\Lambda$ (Equation (2)), which takes place in the (x, z) plane. For normal mode growth, the slope of the perturbation $w/u = (Ro/Br)(v/u)$ is constant, however for non-normal transient growth this slope changes with time. The optimal trajectory of air parcels in the (x, z) plane for the cases of $Ri = 0.1, 0.5, 0.9$ until they converge to the constant slope of the unstable modes is shown in Figure 4 (solid lines). Since the instantaneous growth rate due to Reynolds stress is maximized when the displacement slope is in $\pi/4$ (scaled by Ro/Br) against the shear (indicated by the dashed line), the optimal evolution seeks to pass through this slope at the initial time of evolution.

4. Concluding remarks

We find that symmetric instability can exhibit non-normal growth that can be much larger than predicted by the most unstable mode so that, for instance, the generation of pre-frontal rain bands could occur much quicker than predicted by the modal analysis. While the slope of the parcel trajectory for optimal growth remains close to the isentropes (or to the equivalent isentropes in moist slantwise convection), the difference in this slope, between modal and optimal non-modal evolution, is in the initial

stage and can be seen to be in the plane perpendicular to the isentropes and absolute momentum isolines, where the mean shear is. Furthermore this initial non-modal stage can be a plausible mechanism allowing moist air parcels to reach their level of free slantwise convection, before modal instability is triggered. In general, this triggering perturbation must be externally supplied (e.g. by frontal lifting, or by orography), however for pre-frontal rainbands non-modal lifting can be served as an 'internal' triggering source. This could be yet another way in which non-normal growth can trigger turbulence in a background stable to modal perturbations.

The analysis presented in this note was applied for simplicity for unbounded Boussinesq flow. Recently Xu (2007a,b) conducted a comprehensive thorough analysis of non-modal growth of non-Boussinesq symmetric shear flow, bounded by two horizontal boundaries. He showed that in order to obtain a complete set, one should include in addition of the paired growing and decaying modes two other pairs of slow and fast propagating modes. For instantaneous optimization time, the non-modal growth is produced mainly by the paired fastest propagating modes, whereas for intermediate target time, large growth can be obtained by the paired slowest propagating modes, at the stable side of the marginal stability curve. In the unstable regime, these pairs can also contribute significantly to the energy growth before the fastest-growing mode becomes the dominant component. Since the Boussinesq approximation excludes these mechanisms, it seems to underestimate, especially in the unstable regime, the optimal growth of pre-frontal rainbands.

Xu examined further the different growth mechanisms in terms of the evolution of the different components of the total energy perturbation (i.e. available potential energy, cross-band and along-band kinetic energy). It would be interesting to analyze these results also in terms of the different role of the meridional heat flux and the vertical Reynolds stress sources, and compare it to the analysis presented here for the simpler Boussinesq set-up.

Acknowledgements

The authors are grateful to Qin Xu and Rodrigo Caballero for their thorough reviews and constructive suggestions. EH is grateful to ISF (grant 1084/06) and to the Bi-National Science Foundation BSF (grant 2004087). BF is grateful to NSF ATM-0736022.

References

- Bennetts DA, Hoskins BJ. 1979. Conditional symmetric instability – A possible explanation for frontal rainbands. *Q. J. R. Meteorol. Soc.* **105**: 945–962.
- Emanuel KA. 1983a. The Lagrangian parcel dynamics of moist symmetric stability. *J. Atmos. Sci.* **40**: 2368–2376.
- Emanuel KA. 1983b. On assessing local conditional symmetric instability from atmospheric soundings. *Mon. Weather Rev.* **111**: 2016–2033.
- Farrell BF. 1984. Modal and non-modal baroclinic waves. *J. Atmos. Sci.* **41**: 668–673.
- Farrell BF, Ioannou PJ. 1996. Generalized Stability Theory. Part I: Autonomous operators. *J. Atmos. Sci.* **53**: 2025–2040.
- Heifetz E, Farrell BF. 2003. Generalized Stability of non-geostrophic baroclinic shear flow. Part I: Large Richardson number regime. *J. Atmos. Sci.* **60**: 2083–2100.
- Heifetz E, Farrell BF. 2007. Generalized Stability of non-geostrophic baroclinic shear flow. Part I: Large Richardson number regime. *J. Atmos. Sci.* **64**: 4366–4382.
- Hoskins BJ. 1974. The role of potential vorticity in symmetric stability and instability. *Q. J. R. Meteorol. Soc.* **100**: 480–482.
- Schultz DM, Schumacher PN. 1999. The use and misuse of conditional symmetric instability. *Mon. Weather Rev.* **127**: 2709–2732. Corrigendum **128**: 1573.
- Stone PH. 1966. On non-geostrophic baroclinic stability. *J. Atmos. Sci.* **23**: 390–400.
- Stone PH. 1970. On non-geostrophic baroclinic stability: Part II. *J. Atmos. Sci.* **25**: 721–726.
- Xu Q. 1986a. Conditional symmetric instability and mesoscale rainbands. *Q. J. R. Meteorol. Soc.* **112**: 315–334.
- Xu Q. 1986b. Generalized energetics for linear and nonlinear symmetric instabilities. *J. Atmos. Sci.* **43**: 972–984.
- Xu Q. 2007a. Modal and non-modal symmetric perturbations. Part I: Completeness of normal modes and constructions of non-modal solutions. *J. Atmos. Sci.* **64**: 1745–1763.
- Xu Q. 2007b. Modal and nonmodal symmetric perturbations. Part II: Non-modal growths measured by total perturbation energy. *J. Atmos. Sci.* **64**: 1764–1781.
- Xu Q, Clark JHE. 1985. The nature of symmetric instability and its similarity to convective and inertial instability. *J. Atmos. Sci.* **42**: 2880–2883.
- Xu Q, Zhou XP. 1982. Baroclinic and inertial instability in a non-hydrostatic atmosphere. *Scientia Atmos. Sinica* **6**: 355–367.